Minimizing transient energy growth in plane Poiseuille flow

J F Whidborne[1*], **J McKernan**[2], and **G Papadakis**[2]
[1]Department of Aerospace Science, Cranfield University, Cranfield, UK
[2]King's College London, UK

The manuscript was received on 2 October 2007 and was accepted after revision for publication on 22 January 2008.

DOI: 10.1243/09596518JSCE493

Abstract: The feedback control of laminar plane Poiseuille flow is considered. In common with many flows, the dynamics of plane Poiseuille flow is very non-normal. Consequently, small perturbations grow rapidly with a large transient that may trigger non-linearities and lead to turbulence, even though such perturbations would, in a linear flow, eventually decay. This sensitivity can be measured using the maximum transient energy growth. The linearized flow equations are discretized using spectral methods and then considered at one wave-number pair in order to obtain a model of the flow dynamics in a form suitable for advanced control design. State feedback controllers that minimize an upper bound on the maximum transient energy growth are obtained by the repeated solution of a set of linear matrix inequalities. The controllers are tested using a full Navier–Stokes solver, and the transient energy response magnitudes are significantly reduced compared with the uncontrolled case.

Keywords: flow control, transient energy growth, linear matrix inequality (LMI), Navier–Stokes, plane Poiseuille flow

1 INTRODUCTION

Laminar plane Poiseuille flow (channel flow) is the steady and parallel flow between two infinite parallel planes. Its simple geometry and flow profile means that it serves as a good test case for investigating feedback control for flow systems [**1**–**5**]. Furthermore, plane Poiseuille flow is prone to transition to turbulence even when traditional linear analysis indicates stability. Experiments show that the flow can undergo transition for Reynolds numbers as low as 1000 [**6**], even though the flow is known to be linearly stable at Reynolds numbers below approximately 5772 [**7**]. In common with many other flows, the state equation of plane Poiseuille flow is highly non-normal. After an initial state perturbation, the state trajectories of non-normal systems may exhibit large transients; the occurrence of transition in the linearly stable regime of plane Poiseuille flow is thought to be due to large transient growth causing non-linear effects [**8**–**10**].

The energy of perturbations (or transient energy) is a fundamental notion in the study of turbulence, and is used in this paper as a measure of the size of the perturbations of the state. It has a physical meaning, being the energy density of the velocity perturbations. The system sensitivity is measured by the maximum transient energy growth following some energy-bounded initial state perturbation; this value is critical in determining whether the flow will trigger non-linear effects. The maximum transient energy growth has been studied for a number of fluid systems [**9**, **11**, p. 112]. A comprehensive review of the role of transient energy growth in assessing hydrodynamic stability is provided in reference [**12**].

State feedback control that can minimize an upper bound on the maximum transient energy growth is considered in this paper. The general problem of constraining transient trajectory norms by feedback control has also been considered recently [**13**–**17**]. These approaches all propose minimizing an upper bound on the transient behaviour. The actual

Corresponding author: Department of Aerospace Science, Cranfield University, Cranfield, Beds MK43 0AL, UK. email: j.f.whidborne@cranfield.ac.uk

maximum transient energy growth can be minimized using the methods proposed in references [**18**] and [**19**]. However, these are very computationally expensive, so in this paper an upper bound is minimized, even though the bound may be quite conservative [**17**, p. 668]. The problem of minimizing an upper bound can be solved by the solution of a linear matrix inequality (LMI) problem. An additional LMI is incorporated to constrain the energy of the control effort.

2 PLANE POISEUILLE FLOW

Incompressible fluid flow is described by the Navier–Stokes and continuity equations. The Navier–Stokes equations

$$\dot{\vec{U}} + \left(\vec{U}\cdot\nabla\right)\vec{U} = -\frac{1}{\rho}\nabla P + \frac{\mu}{\rho}\nabla^2\vec{U} \tag{1}$$

form a set of three coupled, non-linear, partial differential equations representing conservation of momentum, where $\vec{U}$ is velocity, P is pressure, ρ is density (uniform), and μ is viscosity (uniform), and the continuity equation

$$\nabla\cdot\vec{U} = 0 \tag{2}$$

is an additional constraint representing the conservation of mass.

Laminar Poiseuille flow, shown in Fig. 1, has a parabolic streamwise velocity profile, with no slip occurring at the bounding parallel planes. It undergoes transition to turbulence when small perturbations $\vec{u} = (u, v, w)$, p about the steady base profile, $\vec{U}_\mathrm{b} = \left(\left(1-(y/h)^2\right)U_\mathrm{cl}, 0, 0\right)$, P_b, grow spatially and temporally to form a self-sustaining turbulent flow. The Navier–Stokes equations for the perturbations

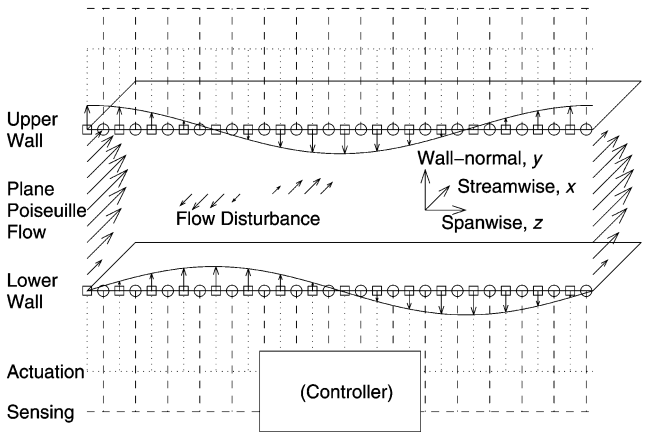

Fig. 1 Plane Poiseuille flow

about the base flow, $\vec{U}_\mathrm{b}$, become

$$\dot{\vec{u}} + (\vec{u}\cdot\nabla)\vec{u} + \left(\vec{U}_\mathrm{b}\cdot\nabla\right)\vec{u} + (\vec{u}\cdot\nabla)\vec{U}_\mathrm{b} = -\frac{1}{\rho}\nabla p + \frac{\mu}{\rho}\nabla^2\vec{u} \tag{3}$$

Assuming the perturbations to be small compared with the base flow, the second-order non-linear term $(\vec{u}\cdot\nabla)\vec{u}$ can be discarded. Non-dimensionalizing equation (3) by dividing length scales by the channel half-height h, dividing velocities by the base centreline velocity U_cl, and dividing pressure by ρU_cl^2 gives

$$\dot{\vec{u}} + \left(\vec{U}_\mathrm{b}\cdot\nabla\right)\vec{u} + (\vec{u}\cdot\nabla)\left(\vec{u}+\vec{U}_\mathrm{b}\right) = -\nabla p + \frac{1}{R}\nabla^2\vec{u} \tag{4}$$

where $R := \rho U_\mathrm{cl} h/\mu$ is the dimensionless Reynolds number. Being linear, the continuity equation (2) simply becomes

$$\nabla\cdot\vec{u} = 0 \tag{5}$$

Fluid flowfield velocity and pressure, and wall shear stresses, can be measured. The flow can be influenced by the manipulation of the conditions on its boundaries, for example by wall transpiration, which is the injection and suction of fluid at the walls. The state of the flow can be determined from shear stress measurements at the walls. Hence, active feedback control of the evolution of transition is feasible. The proposed scheme is shown in Fig. 1. However, equations (4) and (5) are infinite dimensional, so, in order to be able to use standard finite-dimension control methods, and to ensure that the controller is practically implementable, these equations must be approximated by a finite-dimension linear time-invariant system of the form

$$\dot{\boldsymbol{x}} = \mathbf{A}\boldsymbol{x} + \mathbf{B}\boldsymbol{u} \tag{6}$$

$$\boldsymbol{y} = \mathbf{C}\boldsymbol{x} \tag{7}$$

However, a straightforward discretization results in a singular system of the form $\mathbf{E}\dot{\boldsymbol{x}} = \mathbf{A}\boldsymbol{x} + \mathbf{B}\boldsymbol{u}$, where $\mathbf{E}$ is singular. This is a consequence of the algebraic constraint imposed by continuity equation (5), which does not contain pressure.

To proceed, the pressure perturbation term is eliminated from equation (4) by substituting equation (5), giving an expression for the wall-normal velocity

$$\frac{\partial\left(\nabla^2 v\right)}{\partial t} + U_\mathrm{b}\frac{\partial\left(\nabla^2 v\right)}{\partial x} - \frac{\partial^2 U_\mathrm{b}}{\partial y^2}\frac{\partial v}{\partial x} - \frac{1}{R}\nabla^2\left(\nabla^2 v\right) = 0 \tag{8}$$

For a complete description of a three-dimensional flow perturbation, a second equation is required to describe the wall-normal vorticity, η, where

$$\eta = \frac{\partial u}{\partial z} - \frac{\partial w}{\partial x} \tag{9}$$

and equations (4) and (5) give

$$\frac{\partial \eta}{\partial t} + \frac{\partial U_b}{\partial y}\frac{\partial v}{\partial z} + U_b\frac{\partial \eta}{\partial x} - \frac{1}{R}\nabla^2\eta = 0 \tag{10}$$

To implement control by wall transpiration, the no-slip wall boundary conditions at $y = \pm 1$ are replaced with prescribed wall transpiration velocities, $u(\pm 1) = 0$, $v(\pm 1) \neq 0$, $w(\pm 1) = 0$. It is assumed that disturbances on $\vec{u}$ exist in the streamwise (x), wall-normal (y), and spanwise (z) directions. Variations in the wall-normal direction are assumed to be non-periodic and are represented by a modified Chebyshev series that fulfils the wall boundary conditions. Variations in the streamwise and spanwise directions are assumed to have a periodic representation, $\Re(e^{i(\alpha x+\beta z)})$, so flow disturbances grow in time, but not in space. The terms α and β are the streamwise and spanwise wave numbers respectively. Substituting the assumed solutions into equations (8) and (10) and assuming an exponential time variation results in the classical Orr–Sommerfeld and Squire equations respectively.

After some manipulation of the equations, boundary control of the linearized Navier–Stokes equations in a channel at a particular wave-number pair (α, β) (with associated variables denoted by $\widetilde{u}$, $\widetilde{v}$, etc.) can be represented as a linear state-space system in the standard form of equation (6). The linearized Navier–Stokes equations are evaluated at N locations in the wall-normal direction (with the locations more closely spaced near the walls), and the state variables $\boldsymbol{x}$ are the Chebyshev coefficients of the wall-normal velocity, $\widetilde{v}$, and vorticity, $\widetilde{\eta}$, perturbations concatenated with the upper and lower wall $\widetilde{v}$ transpiration velocities. For details, see reference [**20**].

In this paper, state feedback is used, so it is assumed that the system state can be accurately measured. The inputs, $\boldsymbol{u}$, are the rates of change in symmetrical and antisymmetrical components of wall transpiration velocity. Since these are rates of change, the system contains two integrators, with eigenvectors representing symmetrical and antisymmetrical steady state transpiration from the walls. The Chebyshev coefficients are complex, but the state-space system is made real valued by decomposing it into its real- and imaginary-valued parts. The test case considered here is $\alpha = 0$, $\beta = 2.044$, and $R = 5000$. This test case is linearly stable but has the largest transient energy over all unit initial conditions and time and wave-number pairs, and represents the very earliest stages of the transition to turbulence. The model is discretized in the wall-normal direction with $N = 20$. The order of the resulting model is $2N-2$. A 38th-order plant model is high for control purposes, but errors become significant at lower values of N [**20**]. Modelling the turbulence itself would involve using many more degrees of freedom. For a full derivation of the state-space model, see reference [**20**].

3 CONTROL OF TRANSIENT ENERGY GROWTH

Consider the asymptotically stable, linear, time-invariant system described by the initial-value problem

$$\dot{\boldsymbol{x}} = \mathbf{A}\boldsymbol{x}, \qquad \boldsymbol{x}(0) = \boldsymbol{x}_0 \tag{11}$$

with $\mathbf{A} \in \mathbb{R}^{n\times n}$ and $\boldsymbol{x}_0 \in \mathbb{R}^n$, which has the continuous solution $\boldsymbol{x} : \mathbb{R}_+ \to \mathbb{R}^n$, $t \mapsto \boldsymbol{\Phi}(t)\boldsymbol{x}_0$, where $\boldsymbol{\Phi}(t)$ is the state transition matrix given by $\boldsymbol{\Phi}(t) = e^{\mathbf{A}t} = \sum_{i=0}^{\infty} \mathbf{A}^i t^i / i!$.

For simplicity of presentation in this section, the transient energy, $\varepsilon(t)$, is defined as $\varepsilon(t) := \max\{\|\boldsymbol{x}(t)\|^2 : \|\boldsymbol{x}_0\| = 1\}$. The maximum transient energy growth, $\hat{\varepsilon}$, is defined as $\hat{\varepsilon} := \max\{\varepsilon(t) : t \geqslant 0\}$. In practice, the actual transient energy, $\varepsilon(t)$, is

$$\varepsilon(t) = \max\left\{\|\mathbf{W}\boldsymbol{x}(t)\|^2 : \|\mathbf{W}\boldsymbol{x}(0)\| = 1\right\} \tag{12}$$

where $\mathbf{W} > 0$ is a constant weighting matrix that relates the transient energy with the state variables so that the transient energy can be calculated from the norm of the weighted state. Hence, for the remaining results in this section to be applicable to the laminar plane Poiseuille flow problem, a simple change of variables $\widetilde{\boldsymbol{x}} = \mathbf{W}\boldsymbol{x}$ should be performed.

An upper bound, $\hat{\varepsilon}_u \geqslant \hat{\varepsilon}$, of the maximum transient energy growth can be obtained by means of a Lyapunov function that describes an ellipsoid that bounds the trajectory. This upper bound is given by

$$\hat{\varepsilon}_u := \lambda_{\max}(\mathbf{P})\lambda_{\max}\left(\mathbf{P}^{-1}\right) \tag{13}$$

where $\mathbf{P} = \mathbf{P}^T > 0$ satisfies

$$\mathbf{P}\mathbf{A} + \mathbf{A}^T\mathbf{P} < 0 \tag{14}$$

which is the well-known Lyapunov inequality (here, a strict Lyapunov inequality as in reference [**21**] is used, which overcomes some numerical difficulties in the subsequent LMIs [**16**]), and $\lambda_{\max}(\mathbf{P})$ denotes the maximum eigenvalue of $\mathbf{P}$. A proof of the above can be found in reference [**19**].

A minimal upper bound can be obtained by solving the following LMI generalized eigenvalue problem (GEVP) [**22**, p. 65]

$$\min \gamma \text{ subject to } \quad \mathbf{I} \leqslant \mathbf{P} \leqslant \gamma \mathbf{I}, \quad \mathbf{PA} + \mathbf{A}^{\mathrm{T}}\mathbf{P} < 0 \tag{15}$$

where $\mathbf{P} > 0$ is real and symmetric and $\hat{\varepsilon} \leqslant \hat{\varepsilon}_{\mathrm{u}} \leqslant \gamma$.

Now consider the actuated case with the linear time-invariant plant

$$\dot{\boldsymbol{x}} = \mathbf{A}\boldsymbol{x} + \mathbf{B}\boldsymbol{u}, \qquad \boldsymbol{x}(0) = \boldsymbol{x}_0 \tag{16}$$

where $\mathbf{B} \in \mathbb{R}^{n \times \ell}$ and $\boldsymbol{u} : \mathbb{R}_+ \to \mathbb{R}^{\ell}$ is a piecewise continuous function, and with state feedback control $\boldsymbol{u} = \mathbf{K}\boldsymbol{x}$, where $\mathbf{K} \in \mathbb{R}^{\ell \times n}$.

An LMI [**22**, p. 100] can be formulated to obtain a controller that minimizes the upper bound $\hat{\varepsilon}_{\mathrm{u}}$. Expanding inequality (14) for the closed-loop system matrix $\mathbf{A} + \mathbf{BK}$ gives

$$\mathbf{PA} + \mathbf{A}^{\mathrm{T}}\mathbf{P} + \mathbf{PBK} + \mathbf{K}^{\mathrm{T}}\mathbf{B}^{\mathrm{T}}\mathbf{P} < 0 \tag{17}$$

and with the changes in variable, $\mathbf{Q} = \mathbf{P}^{-1}$ and $\mathbf{Y} = \mathbf{KQ}$, the LMI

$$\mathbf{AQ} + \mathbf{QA}^{\mathrm{T}} + \mathbf{BY} + \mathbf{Y}^{\mathrm{T}}\mathbf{B}^{\mathrm{T}} < 0 \tag{18}$$

is obtained. Now, because $\lambda_{\max}(\mathbf{P})\lambda_{\max}(\mathbf{P}^{-1}) = \lambda_{\max}(\mathbf{Q})\lambda_{\max}(\mathbf{Q}^{-1})$, it is possible to obtain a controller that minimizes the upper bound of the maximum transient energy growth by solving the following LMI generalized eigenvalue problem (GEVP)

$$\begin{aligned} &\min \gamma \text{ subject to } \quad \mathbf{I} \leqslant \mathbf{Q} \leqslant \gamma \mathbf{I} \\ &\mathbf{AQ} + \mathbf{QA}^{\mathrm{T}} + \mathbf{BY} + \mathbf{Y}^{\mathrm{T}}\mathbf{B}^{\mathrm{T}} < 0 \end{aligned} \tag{19}$$

and the upper-bound minimizing controller is $\mathbf{K} = \mathbf{YQ}^{-1}$.

For a practical design, it is necessary to limit the expenditure of control effort. This can be done by simultaneously solving the above LMI with one described in reference [**22**, p. 103] as follows. A norm on the control input $\boldsymbol{u}(t) = \mathbf{K}\boldsymbol{x}(t)$ is

$$\max_{t \geqslant 0} \|\boldsymbol{u}(t)\|^2 = \max_{t \geqslant 0} \left\|\mathbf{YQ}^{-1}\boldsymbol{x}(t)\right\|^2 \tag{20}$$

If $\mathbf{Q}$ and $\mathbf{Y}$ satisfy problem (19) and $\boldsymbol{x}(0)^{\mathrm{T}}\mathbf{Q}^{-1}\boldsymbol{x}(0) \leqslant 1$, then, as $\boldsymbol{x}$ satisfies $\boldsymbol{x}^{\mathrm{T}}\mathbf{Q}^{-1}\boldsymbol{x} \leqslant \boldsymbol{x}(0)^{\mathrm{T}}\mathbf{Q}^{-1}\boldsymbol{x}(0)$ for all $t \geqslant 0$, it follows that

$$\max_{t \geqslant 0} \|\boldsymbol{u}(t)\|^2 \leqslant \max_{\boldsymbol{x}^{\mathrm{T}}\mathbf{Q}^{-\frac{1}{2}}\mathbf{Q}^{-\frac{1}{2}}\boldsymbol{x} < 1} \left\|\mathbf{YQ}^{-\frac{1}{2}}\mathbf{Q}^{-\frac{1}{2}}\boldsymbol{x}\right\|^2 \tag{21}$$

The induced 2-norm is equal to the largest singular value

$$\max_{t \geqslant 0} \|\boldsymbol{u}(t)\|^2 \leqslant \lambda_{\max}\left(\mathbf{Q}^{-\frac{1}{2}}\mathbf{Y}^{\mathrm{T}}\mathbf{YQ}^{-\frac{1}{2}}\right) \tag{22}$$

Hence, a constraint

$$\max_{t \geqslant 0} \|\boldsymbol{u}(t)\|^2 \leqslant \mu^2 \tag{23}$$

can be obtained by a solution of the LMIs

$$\begin{bmatrix} 1 & \boldsymbol{x}(0)^{\mathrm{T}} \\ \boldsymbol{x}(0) & \mathbf{Q} \end{bmatrix} \geqslant 0, \qquad \begin{bmatrix} \mathbf{Q} & \mathbf{Y}^{\mathrm{T}} \\ \mathbf{Y} & \mu^2\mathbf{I} \end{bmatrix} \geqslant 0 \tag{24}$$

Furthermore, the constraint on the initial conditions $\boldsymbol{x}(0)^{\mathrm{T}}\mathbf{Q}^{-1}\boldsymbol{x}(0) \leqslant 1$ can be replaced with the constraint $\boldsymbol{x}(0)^{\mathrm{T}}\boldsymbol{x}(0) \leqslant 1$, providing it is more restrictive. The sphere $\boldsymbol{c}^{\mathrm{T}}\boldsymbol{c} = 1$ lies within the ellipse $\boldsymbol{c}^{\mathrm{T}}\mathbf{Q}^{-1}\boldsymbol{c} = 1$ if the shortest ellipse semi-axis of $\mathbf{Q}^{-1}$ is greater than or equal to 1, i.e. $1 \Big/ \sqrt{\lambda_{\max}\left(\mathbf{Q}^{-1}\right)} \geqslant 1$. Thus, the system of LMIs to be solved to restrict the control effort to μ^2 from initial conditions $\boldsymbol{x}(0)^{\mathrm{T}}\boldsymbol{x}(0) \leqslant 1$ becomes

$$\mathbf{Q} \geqslant \mathbf{I}, \qquad \begin{bmatrix} \mathbf{Q} & \mathbf{Y}^{\mathrm{T}} \\ \mathbf{Y} & \mu^2\mathbf{I} \end{bmatrix} \geqslant 0 \tag{25}$$

The complete LMI problem to stabilize the system, minimize the upper bound of the transient growth, and limit the control effort becomes

$$\begin{aligned} &\min \gamma \text{ subject to } \quad \mathbf{I} \leqslant \mathbf{Q} \leqslant \gamma \mathbf{I} \\ &\mathbf{AQ} + \mathbf{QA}^{\mathrm{T}} + \mathbf{BY} + \mathbf{Y}^{\mathrm{T}}\mathbf{B}^{\mathrm{T}} < 0, \quad \begin{bmatrix} \mathbf{Q} & \mathbf{Y}^{\mathrm{T}} \\ \mathbf{Y} & \mu^2\mathbf{I} \end{bmatrix} \geqslant 0 \end{aligned} \tag{26}$$

Note that a constraint on the rate of transient decay can be simultaneously incorporated into this expression [**13**].

4 RESULTS AND SIMULATIONS

The transient energy $\varepsilon(t)$ of the linearized system with no wall transpiration is shown in Fig. 2, and has a maximum transient energy growth $\hat{\varepsilon} = 4941$. This value differs slightly (by less than 1 per cent) from the

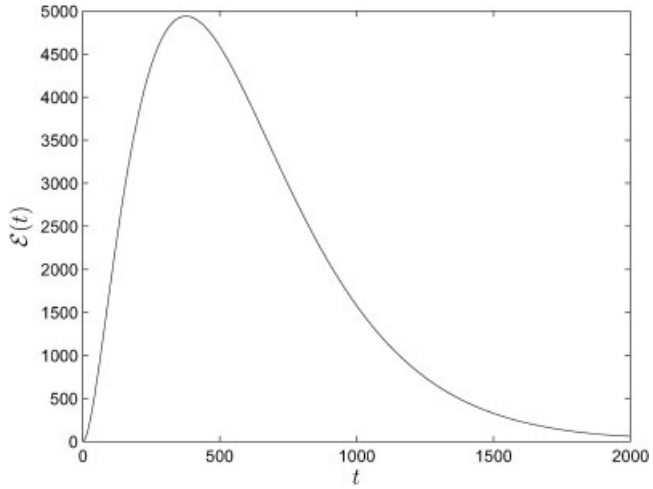

Fig. 2 Transient energy for system with no transpiration

value given in reference [**23**] of $\hat{\varepsilon} = 4897$, owing to the approximations made with $N = 20$. For larger values of N, the LMI problem becomes difficult to solve.

The problem is first solved without any restriction on the control effort, that is, a controller that satisfied problem (19) was obtained. The upper bound is $\hat{\varepsilon}_u = 1722$. The transient energy $\varepsilon(t)$ is shown in Fig. 3. The actual maximum transient energy growth is $\hat{\varepsilon} = 883$. There is quite a large gap between the upper bound and the actual value, as noted in reference [**17**, p. 668]. As expected, the control gains are impractically large, with the largest control gain element being max $|\mathbf{K}| = 776.5 \times 10^3$.

The effect of including the constraint on the control signal (23) is investigated next. Problem (26) is solved for a range of values of μ. The resulting $\hat{\varepsilon}_u$ and corresponding $\hat{\varepsilon}$ are shown in Fig. 4. Interestingly, $\hat{\varepsilon}$ is not lowest when μ is greatest. This was also seen for the Lorenz equation control system studied in reference [**24**]. In fact, minimal $\hat{\varepsilon}$ occurs for $\mu \simeq 20$. For $\mu = 20$, the upper bound is $\hat{\varepsilon}_u = 1722$ and is only marginally greater than the minimal value. The actual maximum transient energy growth is $\hat{\varepsilon} = 825$, and the transient energy $\varepsilon(t)$ is shown in Fig. 5. The largest control gain element is max $|\mathbf{K}| = 13.64$. Figure 6 shows the worst-case wall control $\boldsymbol{u}_{wc} = \mathbf{K}\boldsymbol{x}_{wc}$, where $\boldsymbol{x}_{wc}$ is the transient $\boldsymbol{x}(t)$ that results in the largest energy gain. Note that the second control signal is zero. The details are discussed in references [**20**] and [**25**].

The control effort can be substantially reduced without a significant performance deterioration by setting $\mu = 0.8$. The transient energy $\varepsilon(t)$ is shown in Fig. 7, and the actual maximum transient energy growth is $\hat{\varepsilon} = 842$. Figure 8 shows the worst-case wall control $\boldsymbol{u}_{wc}$. Again, note that the second control signal is zero. Both the control signal magnitudes and the control gains are small, with the largest control gain element max $|\mathbf{K}| = 0.558$.

A finite-volume computational fluid dynamics (CFD) Navier–Stokes solver is used for non-linear simulation of the system. This solver makes no assumption of spectral behaviour, solves the full non-linear Navier-Stokes equations, and is completely independent of the spectral code used for the controller synthesis and linear simulations. The full Navier–Stokes solver employs an unstructured, collocated grid, and is capable of representing complex geometry, for example as utilized in reference [**26**], although a simple structured mesh of the channel is

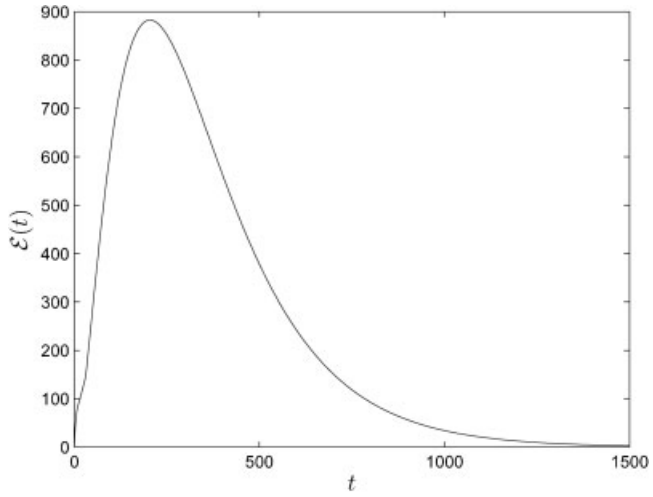

Fig. 3 Transient energy for minimal upper-bound controller with unlimited control effort

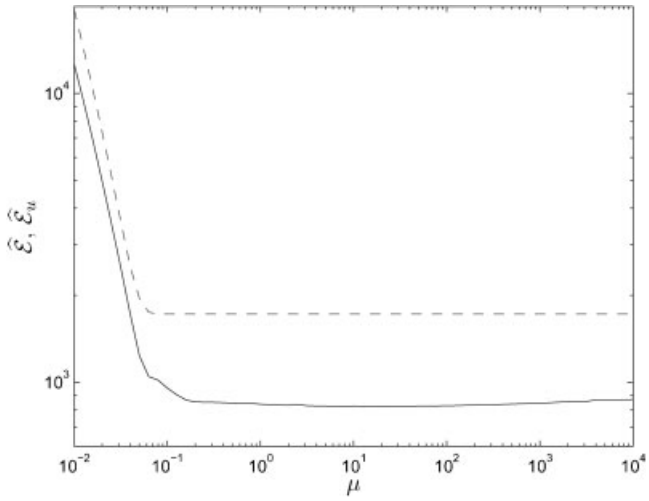

Fig. 4 Maximum transient energy growth upper bound $\hat{\varepsilon}_u$ (dashed line) and actual maximum transient energy growth $\hat{\varepsilon}$ (solid line) versus control effort constraint μ (log scale)

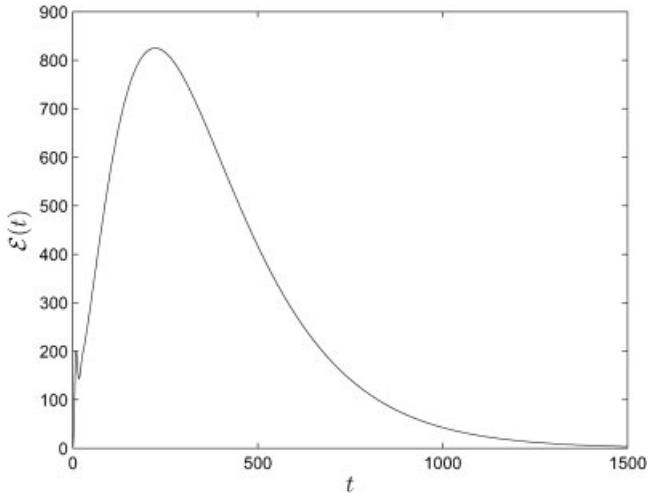

Fig. 5 Transient energy for minimal upper-bound controller with control effort constraint $\mu = 20$

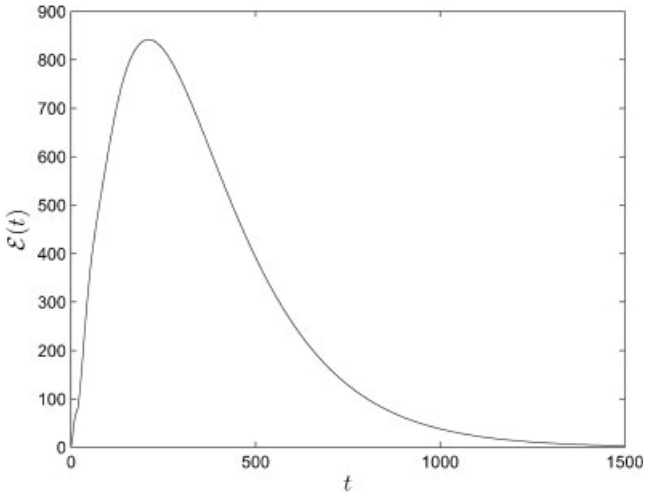

Fig. 7 Transient energy for minimal upper-bound controller with control effort constraint $\mu = 0.8$

used in the present work. A second-order central differencing scheme is used to discretize the spatial terms, and a first-order Euler implicit scheme is used for time marching. See reference [**20**] for further details.

In order to perform comparative assessment of the CFD results, a datum perturbation energy for the initial condition is defined. The value is set at $\|\widetilde{\boldsymbol{x}}_0\|^2 = E_c = 2.26 \times 10^{-9}$. This value is 8.5×10^{-9} of the base-flow energy density and is approximately 1/100th of the open-loop streamwise vortex transition threshold of 2.56–2.65×10^{-7} as determined by Reddy *et al.* [**27**, p. 292]. From the linear model, the initial conditions that result in the 'worst-case' response are determined, i.e. the initial conditions such that the resulting state response $\widetilde{\boldsymbol{x}}_{wc}(t)$ satisfies $\max\{\|\widetilde{\boldsymbol{x}}_{wc}(t)\|^2 : t \geqslant 0\} = \hat{\varepsilon}$. Here, the response energy from these initial conditions, $\|\widetilde{\boldsymbol{x}}_{wc}(t)\|^2$, is called the *worst-case response energy*. The worst-case response energy with initial energy 10^4 E_c for the uncontrolled flow is shown in Fig. 9 (labelled 'Linear'), along with the corresponding response energy from the same worst-case initial conditions obtained from the CFD simulation (labelled 'Non-linear'). The peak linear response energy is over 4 times greater than the non-linear CFD response energy. At $t \simeq 120$ the energy peaks, indicating that the CFD simulated flow has saturated.

The minimal upper-bound controller with control effort constraint $\mu = 0.8$ is considered next. The worst-case response energy with initial energy E_c is

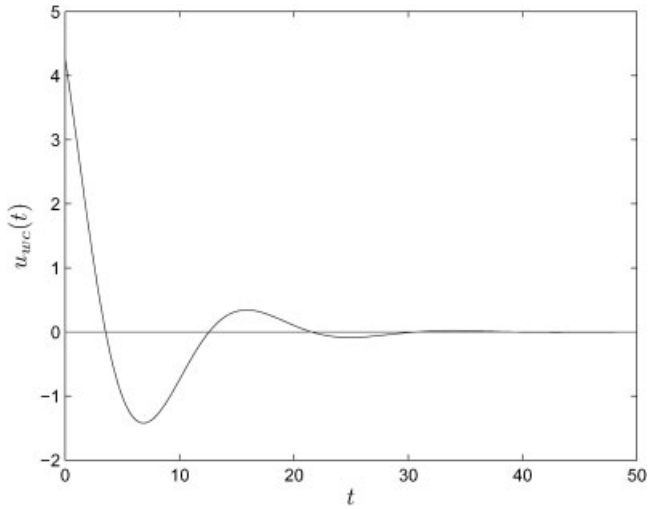

Fig. 6 Worst-case wall control for minimal upper-bound controller with control effort constraint $\mu = 20$

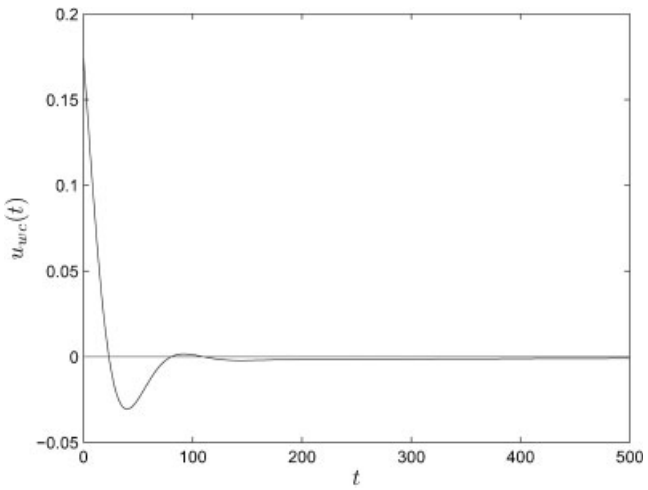

Fig. 8 Worst-case wall control for minimal upper-bound controller with control effort constraint $\mu = 0.8$

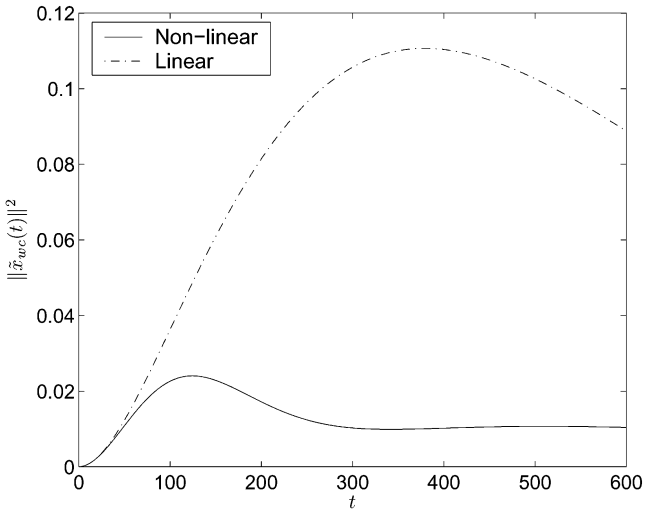

Fig. 9 Worst-case response energy for uncontrolled flow with initial energy 10^4 E_c

shown in Fig. 10, along with the corresponding response from the CFD simulation. The responses are very close, showing that the linear approximation is good, and that the states have remained in the linear region. The worst-case response energy with initial energy 10^4 E_c is shown in Fig. 11. The non-linear response saturates, but the peak is far less than the open-loop response energy from the same initial condition energy shown in Fig. 9.

5 CONCLUDING COMMENTS

The minimization of an upper bound of the maximum transient energy growth of plane Poiseuille

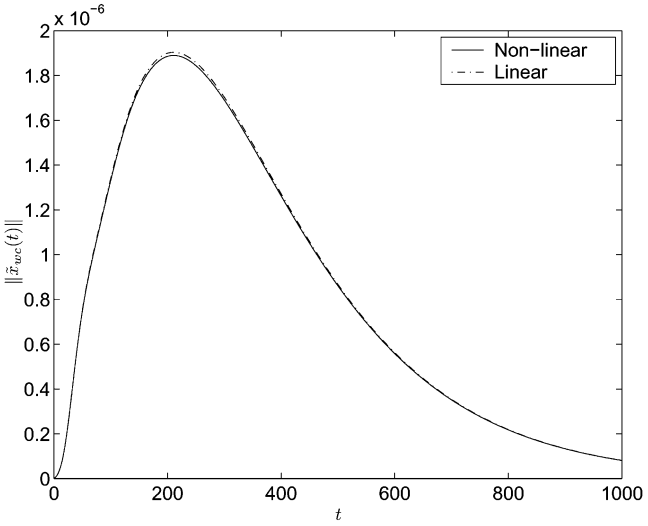

Fig. 10 Worst-case response energy for minimal upper-bound controller with control effort constraint $\mu = 0.8$ with initial energy E_c

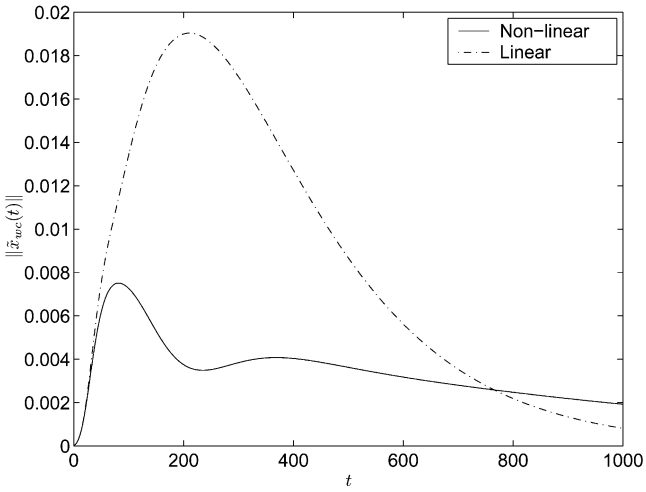

Fig. 11 Worst-case response energy for minimal upper-bound controller with control effort constraint $\mu = 0.8$ with initial energy 10^4 E_c

flow by state-variable feedback has been considered. A periodicity assumption on the flow velocity field is made, and the controllers are designed for a single wave-number pair. This assumption has practical limitations; control of non-periodic plane Poiseuille flow has been tackled in reference [**28**]. The derived linear model has a higher order than is usual for control design. Devising model order reduction methods that retain the modes that are significant for stability and high transient energy growth remains for future work.

Although $\mathcal{H}_\infty$-, $\mathcal{H}_2$-, and $\mathcal{L}_1$-based measures are usually preferred for control system design [**29**], transient energy is useful in fluid flow control because it is relatively easy to verify through CFD simulation. The use of $\mathcal{H}_\infty$ and $\mathcal{H}_2$ norms as stability measures for fluid flow systems is discussed in detail in reference [**4**].

Methods have been devised to minimize the actual maximum transient energy growth rather than the upper bound [**18**, **30**], but these are very computationally intensive and result in very high-order controllers. The phenomenon of high transient energy growth is often a symptom of non-normality, a property of many fluid flow systems. It is envisaged that the approach used here will be suitable for analysing and designing linear control systems for any fluid control system that is very non-normal.

REFERENCES

1 **Joshi, S. S., Speyer, J. L.,** and **Kim, J.** A systems theory approach to the feedback stabilization of infinitesimal and finite-amplitude disturbances in

plane Poiseuille flow. *J. Fluid Mechanics*, 1997, **332**(4), 157–184.
2 **Bewley, T. R.** and **Liu, S.** Optimal and robust control and estimation of linear paths to transition. *J. Fluid Mechanics*, 1998, **365**, 305–349.
3 **Baramov, L., Tutty, O. R.,** and **Rogers, E.** Robust control of linearised Poiseuille flow. *J. Guidance, Control, and Dynamics*, 2002, **25**(1), 145–151.
4 **Jovanović, M. R.** and **Bamieh, B.** Componentwise energy amplification in channel flows. *J. Fluid Mechanics*, July 2005, **534**, 145–183.
5 **McKernan, J., Whidborne, J. F.,** and **Papadakis, G.** Linear quadratic control of plane Poiseuille flow – the transient behaviour. *Int. J. Control*, 2007, **80**(12), 1912–1930.
6 **Carlson, D. R., Widnall, S. E.,** and **Peeters, M. F.** A flow-visualization study of transition in plane Poiseuille flow. *J. Fluid Mechanics*, 1982, **121**, 487–505.
7 **Orszag, S. A.** Accurate solution of the Orr–Sommerfeld stability equation. *J. Fluid Mechanics*, 1971, **50**(4), 689–703.
8 **Farrell, B. F.** Optimal excitation of perturbations in viscous shear flow. *Phys. Fluids*, 1988, **31**(8), 2093–2102.
9 **Reddy, S. C.** and **Henningson, D. S.** Energy growth in viscous channel flows. *J. Fluid Mechanics*, 1993, **252**, 209–238.
10 **Trefethen, L. N., Trefethen, A. E., Reddy, S. C.,** and **Driscoll, T. A.** Hydrodynamic stability without eigenvalues. *Science*, 1993, **261**, 578–584.
11 **Schmid, P. J.** and **Henningson, D. S.** *Stability and transition in shear flows*, vol. 142 of Applied Mathematical Sciences series, 2001 (Springer, New York).
12 **Schmid, P. J.** Nonmodal stability theory. *Annual Rev. Fluid Mechanics*, 2007, **39**, 129–162.
13 **Hinrichsen, D., Plischke, E.,** and **Wirth, F.** State feedback stabilization with guaranteed transient bounds. In Proceedings of the 15th International Symposium on *Mathematical Theory of Networks and Systems*, South Bend, Indiana, August 2002, CDROM, paper 2132.
14 **Plischke, E.** and **Wirth, F.** Stabilization of linear systems with prescribed transient bounds. In Proceedings of the 16th International Symposium on *Mathematical Theory of Networks and Systems (MTNS2004)*, Leuven, Belgium, July 2004.
15 **Wirth, F.** Transient behavior and robustness. In Proceedings of the 16th International Symposium on *Mathematical Theory of Networks and Systems (MTNS2004)*, Leuven, Belgium, July 2004.
16 **Plischke, E.** *Transient effects of linear dynamical systems*, PhD Thesis, Universität Bremen, 2005.
17 **Hinrichsen, D.** and **Pritchard, A. J.** *Mathematical systems theory I: modelling, state space analysis, stability and robustness*, vol. 48 of Texts in Applied Mathematics series, 2005 (Springer, Berlin).
18 **Whidborne, J. F., McKernan, J.,** and **Steer, A. J.** Minimization of maximum transient energy growth by output feedback. In Proceedings of the 16th IFAC World Congress, Prague, July 2005.
19 **Whidborne, J. F.** and **McKernan, J.** On minimizing maximum transient energy growth. *IEEE Trans. Autom. Control*, September 2007, **52**(9), 1762–1767.
20 **McKernan, J.** *Control of plane Poiseuille flow: a theoretical and computational investigation*, PhD Thesis, Cranfield University, 2006.
21 **Skelton, R. E., Iwasaki, T.,** and **Grigoriadis, K. M.** *A unified algebraic approach to linear control design*, 1998 (Taylor and Francis, London).
22 **Boyd, S., El Ghaoui, L., Feron, E.,** and **Balakrishnan, V.** *Linear matrix inequalities in system and control theory*, 1994 (SIAM, Philadelphia, Pennsylvania).
23 **Butler, K. M.** and **Farrell, B. F.** Three-dimensional optimal perturbations in viscous shear flow. *Phys. Fluids A*, 1992, **4**, 1637.
24 **McKernan, J., Whidborne, J. F.,** and **Papadakis, G.** Minimisation of transient perturbation growth in linearised Lorenz equations. In Proceedings of the 16th IFAC World Congress, Prague, July 2005.
25 **Whidborne, J. F., McKernan, J.,** and **Papadakis, G.** Minimal transient energy growth for plane Poiseuille flow. In Proceedings of the UKACC International Control Conference 2006 (ICC2006), Glasgow, UK, August 2006, CDROM, paper 189.
26 **Yeoh, S. L., Papadakis, G.,** and **Yianneskis, M.** Large eddy simulation of turbulent flow in a Rushton impeller stirred reactor with sliding-deforming mesh methodology. *Chem. Engng Technol.*, 2004, **27**(3), 257–263.
27 **Reddy, S. C., Schmid, P. J., Baggett, J. S.,** and **Henningson, D. S.** On stability of streamwise streaks and transition thresholds in plane channel flows. *J. Fluid Mechanics*, 1998, **365**, 269–303.
28 **Baramov, L., Tutty, O. R.,** and **Rogers, E.** $\mathcal{H}_\infty$ control of nonperiodic two-dimensional channel flow. *IEEE Trans. Control Syst. Technol.*, 2004, **12**(1), 111–122.
29 **Doyle, J. C., Francis, B. A.,** and **Tannenbaum, A. R.** *Feedback control theory*, 1991 (Macmillan, New York).
30 **Whidborne, J. F., McKernan, J.,** and **Steer, A. J.** On minimizing maximum transient energy growth, CoA report 0501, Cranfield University, Cranfield, UK, June 2005.

APPENDIX

Notation

A	system matrix
B	input matrix
C	output matrix
E_c	initial perturbation energy
$\vec{f}$	Cartesian vector $(f_x\vec{i}+f_y\vec{j}+f_z\vec{k})$
$\dot{f}$	differentiation of f with respect to time t
∇f	grad $f = (\partial f/\partial x, \partial f/\partial y, \partial f/\partial z)$

$\nabla\cdot\vec{f}$	$\mathrm{div}\,\vec{f}=\left(\partial f_x/\partial x+\partial f_y/\partial y+\partial f_z/\partial z\right)$
h	channel half-height
$\mathbf{K}$	state feedback matrix
p	small pressure perturbation
P	pressure
P_{b}	steady base-flow pressure
R	Reynolds number
$\Re(\cdot)$	real part of a complex number
t	time
$\boldsymbol{u}$	control vector
$\boldsymbol{u}_{\mathrm{wc}}$	worst-case wall control
$\vec{\boldsymbol{u}}=(u, v, w)$	vector of small flow perturbation velocities in the (x, y, z) directions
$(\widetilde{u}, \widetilde{v}, \widetilde{w})$	(u, v, w) Fourier coefficients at the wave number pair (α, β)
U_{cl}	base flow centre-line velocity
$\vec{U}$	flow velocity
$\vec{U}_{\mathrm{b}}$	steady base-flow velocity (parabolic profile)
x, y, z	streamwise, wall-normal, and spanwise coordinates respectively
$\widetilde{\boldsymbol{x}}$	state-variable (weighted) vector
$\widetilde{\boldsymbol{x}}_{\mathrm{wc}}$	worst-case state-variable (weighted) response
$\mathbf{X}>0$ $(\mathbf{X}\geqslant 0)$	symmetric matrix $\mathbf{X}$ is positive definite (semi-definite)
$\boldsymbol{y}$	output vector
α	wave number in the streamwise (x) direction
β	wave number in the spanwise (z) direction
$\varepsilon(t)$	transient energy at time t
$\hat{\varepsilon}$	maximum transient energy growth
$\hat{\varepsilon}_{\mathrm{u}}$	upper bound of the maximum transient energy growth
η	small wall-normal vorticity perturbation
$\widetilde{\eta}$	η Fourier coefficient at the wave-number pair (α, β)
$\lambda_{\max}(\mathbf{X})$	maximum eigenvalue of the symmetric real matrix $\mathbf{X}$
μ	viscosity (uniform)
ρ	density (uniform)